Article
Vol. 25, No. 2, p. 93–105, April 2021
https://doi.org/10.1007/s12303-020-0008-9
pISSN 1226-4806 eISSN 1598-7477
Geosciences Journal GJ

# Latest Quaternary mass-transport processes of fan-shaped body in the western margin of the Ulleung Basin, East Sea (Japan Sea)

Sang-Hoon Lee[1,2]*, Hyeong-Tae Jou[1], Jang-Jun Bahk[3], Hyunggu Jun[1], Seong-Hoon Moon[1,2], Han-Joon Kim[1,2], Senay Horozal[3], Deniz Cukur[4], In-Kwon Um[4], Dong-Geun Yoo[4], and Roger Urgeles[5]

[1]Marine Active Fault Research Center, Korea Institute of Ocean Science and Technology, Busan 49111, Republic of Korea
[2]KIOST School, University of Science and Technology, Daejeon 34113, Republic of Korea
[3]Department of Oceanography and Ocean Environmental Sciences, Chungnam National University, Daejeon 34134, Republic of Korea
[4]Petroleum and Marine Research Division, Korea Institute of Geoscience and Mineral Resources, Daejeon 34132, Republic of Korea
[5]Department de Geociències Marines, Institute de Ciències del Mar (CSIC), Pg. Marítim de la Barceloneta, 37-49, 08003 Barcelona, Spain

**ABSTRACT:** In the western margin of the Ulleung Basin, a detailed analysis of cores with geophysical data from a fan-shaped body, just downslope of a submarine gully associated upslope with failure scars, reveals various modes of mass-transport processes. The arcuate failure scars occurs in water depths exceeding 600 m. The fan-shaped body, less than ca. 10 km long in radius, displays strong back-scatter intensity in sonar images, and corresponds to the uppermost transparent mass in Chirp sub-bottom profiles. Sediment cores penetrating to the uppermost transparent mass consist mostly of various facies of mass-transport deposits (MTDs), causing the strong back-intensity in the sonar images. The interval of MTD facies comprises the upper and lower units without hemi-pelagic muds between them, implying that the fan-shaped body was probably deposited during a single event separated in at least two stages without a significant time break. The lower unit shows brittle to plastic deformation of soft muds (slides/slumps), whereas the upper units exhibits fully fragmented soft mud clasts (low viscous debris flows). Both the upper and lower units involve same original lithology (i.e., soft hemi-pelagic mud) prior to failures, suggesting that the lithology could not significantly affect depositional processes. The fully fragmented soft mud clasts of the upper unit are probably indicative of more shearing than the brittle to plastic deformation of soft muds in the lower unit. Considering the small dimension of the failure scars/gully and the same original lithology, the more shearing of the upper unit was most likely caused by longer transport distance than that of the lower unit. The rare turbidites with absence of channel-levee systems in the fan-shaped body and the failure scars confined in the upper to middle slopes suggest that the submarine gully probably formed by slope failures, not by erosion of turbidity currents.

**Key words:** mass-transport processes, mass-transport deposits, slope failures, late Quaternary, Ulleung Basin (East Sea)

Manuscript received April 18, 2019; Manuscript accepted March 2, 2020

## 1. INTRODUCTION

Submarine slope failures are very common phenomena in worldwide continental margins, flanks of volcanic islands/ridges, fjords, and prodelta slopes (Hampton et al., 1996; Chough et al., 1997; McAdoo et al., 2000; Locat and Lee, 2002; Masson et al., 2002). Reworked sediments from these slope failures generally move downslope through diverse transfer pathways (e.g., submarine gully, valley, canyon, etc.), forming various styles of mass-transport deposits (MTDs) at/near the base of slope in the continental margin (Piper et al., 1985; Walker, 1992; Masson et al., 2006; Elverhoi et al., 2010; Saller et al., 2012; Lee et al., 2014). The characteristics of mass-transport deposits (MTDs) have therefore provided important clues for understanding the characters of slope failures (e.g., style, volume, area of failure, lithology of failed mass, etc.) and the mode/process of downslope transport of the failed masses (Tripsanas et al., 2008; Lee et al., 2013; Bahk et al., 2017).

The Ulleung Basin is characterized by the extensive occurrence of late Quaternary MTDs along the basin margin (Chough et al., 1997; Lee et al., 2004). Slides/slumps and debris-flow deposits

*Corresponding author:
Sang-Hoon Lee
Marine Active Fault Research Center, Korea Institute of Ocean Science and Technology, Busan 49111, Republic of Korea
Tel: +82-51-664-3503, E-mail: sanglee@kiost.ac.kr

typically occur on the middle to lower slopes, whereas turbidites are present on the basin plain (Fig. 1). In the western margin of the Ulleung Basin, several arcuate failure scars located seaward of the shelf break occur in water depth exceeding 600 m, and connect downslope to a submarine gully (Fig. 2a). On the base-of-slope just downslope of the gully mouth, strong back-scatter intensity of a small-scale (less than ca. 10 km in radius) fan-shaped body is observed in long-range side-scan sonar images (Fig. 2b). This study describes acoustic and morphologic features of the fan-shaped body using long-range side-scan sonar images and sub-bottom profiles, and analyzes in detail lithologic characters of core sediments from the fan-shaped body. The aim of the study is to provide a better understanding of the mass-transport processes that formed the small-scale fan-shaped body at the foot of the slope and to characterize the mode of downslope transfer of the failed masses.

## 2. GEOLOGIC SETTING

The Ulleung Basin is a semi-enclosed back-arc basin bordered by the Korea Plateau, the eastern margin of the Korean Peninsula, the Japanese Arc, and the Oki Bank. The basin is bounded by a narrow (less than 25 km wide) shelf and rather steep (4–10°) slope in the western margin. In the shelf, the N-S-oriented topographic high (Hupo Bank) and low (Hupo Trough) are present (Fig. 1). The Hupo Trough is more than ca. 150 m deep, and the Hupo Bank, about 85 km long, rises more than 100 m above the surrounding seafloor. In the southern and eastern margins, the Ulleung Basin is flanked by a broad (30–150 km wide) shelf and relatively gentle (< 2°) slope (Fig. 1). The northeastern part of the basin is punctuated by volcanic islands (Ulleung and Dok islands) and seamounts. The basin plain deepens northeastward, up to about 2300 m deep, connecting to the Japan Basin through

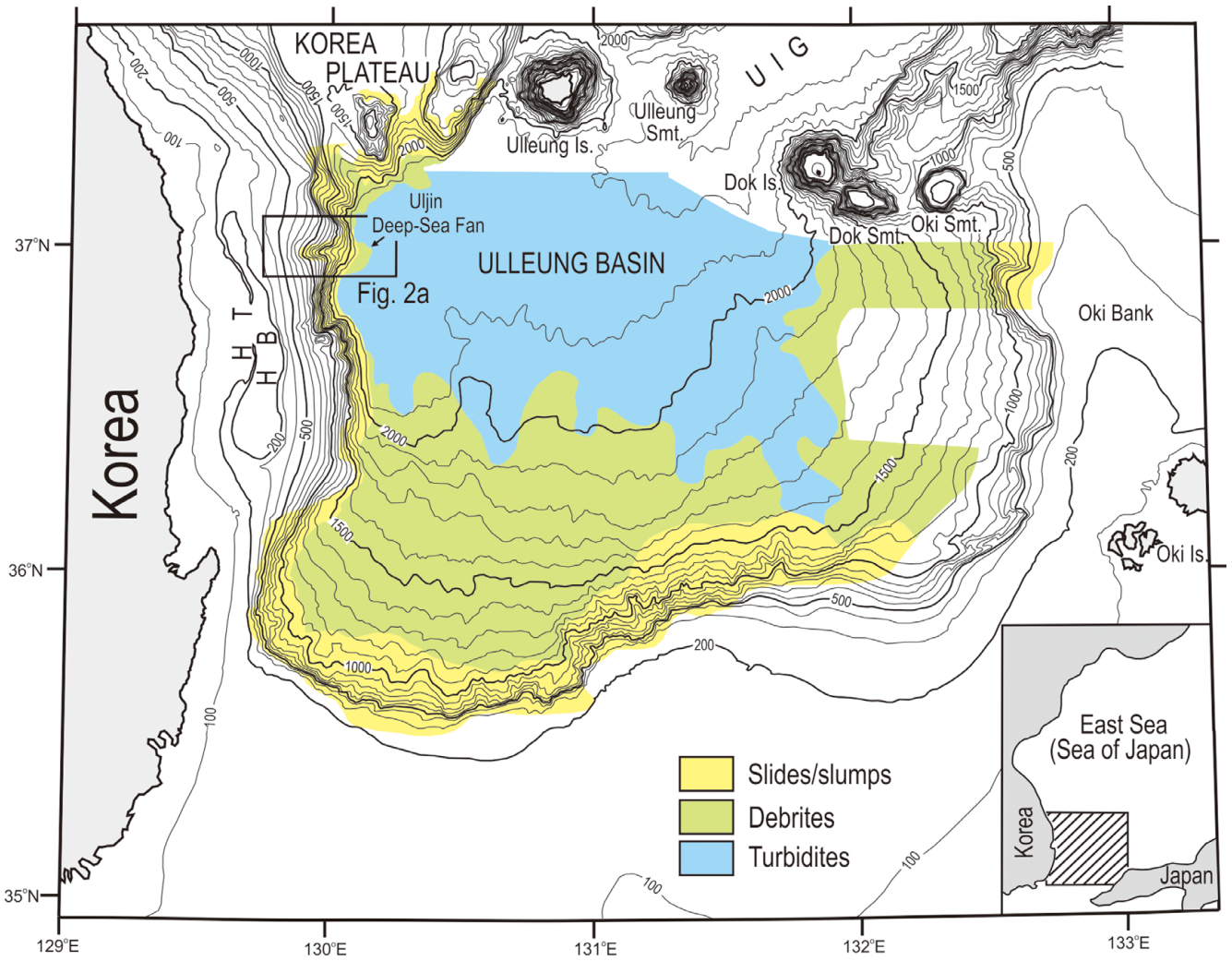


**Fig. 1.** Physiography of the Ulleung Basin and adjacent areas in the East Sea. Zonal distribution of late Quaternary slides/slumps, debris-flow deposits and turbidites identified from Chirp (2–7 kHz) sub-bottom profiles (Lee et al., 1999, 2004). Water depths in meters. HB = Hupo Bank; HT = Hupo Trough; Is. = Island; Smt. = seamount; UIG = Ulleung Interplain Gap.

https://doi.org/10.1007/s12303-020-0008-9 https://www.springer.com/journal/12303

the Ulleung Interplain Gap.

In Chirp (2–7 kHz) sub-bottom profiles, the uppermost sedimentary sequence (ca. 20–30 m thick below the seafloor) displays that late Quaternary MTDs occur in a series of contour-parallel belts (Chough et al., 1997; Lee et al., 2004). On the upper to middle slopes, slide and slump deposits are present, whereas debrites and turbidites are dominant on the lower slope and basin plain, respectively (Fig. 1). The zonal distribution of MTDs implies that those were most likely sourced from regional sediment failures with large-scale transformation from slides and slumps to turbidity currents through debris flows (Chough et al., 1997; Lee et al., 1999). The late Quaternary slope failures were most likely triggered by combinations involving earthquakes, sea-level lowering and gas-hydrate dissociation (Lee et al., 2004, 2013; Cukur et al., 2016).

Late Quaternary MTDs and slope failures in the western and southern margins of the Ulleung Basin show contrasting styles (Lee et al., 2014). On the western margin, a few small-scale, isolated scoop-shaped scars or gullies occur in water depths exceeding 500–700 m (Fig. 1). The downslope MTDs are present as small, solitary masses restricted to the base-of-slope. In contrast, the southern margin displays large-scale, gullied scars from ca. 250 m in water depth. These sediment failures are bounded downslope by extensive occurrence of debrites and turbidites that are not restricted only to the lower slope, but further to the basin plain (Fig. 1). The contrasting styles in MTDs and slope failures of the western and southern margins of the Ulleung Basin are inferred to result from differences in sediment type and supply to the slope during sea-level lowstands (Lee et al., 2014).

## 3. DATA AND METHODS

In order to document morphologic features, bathymetric data and long-range side-scan sonar images were used. Bathymetric data were collected using multi-beam echo sounding systems (KORNSBERG EM 120 and EM302). Post-processing of the data was performed using CARIS HIPS & SIPS software. Side-scan sonar images were collected using the HAWAII Mapping Researcher (MR-1) system by the U.S. Naval Research Laboratory and the Korea Navy (Gardner et al., 1998; Lee et al., 2013). The MR-1 system is a wide-swath (7.5 times the water depth) side-scan sonar system (11–12 kHz) that obtains back-scattering imagery in full ocean depths. Detailed post-processing of the sonar data was described in Gardner et al. (1998).

For providing geometry and internal acoustic characters of the uppermost sedimentary sequence (about 50–60 m thick below the seafloor), high-resolution sub-bottom profiles were acquired using a Chirp sub-bottom profiling system (Benthos Chirp III). The system emitted a frequency of 2–7 kHz band as a source signal. Returned signals were processed by a matched-filtered correlation to record the band of 2–7 kHz, resulting in higher resolution images than those of 3.5 kHz system.

In 2015 and 2016, four piston cores (322–719 cm long) were obtained from a fan-shaped body at the base-of-slope in the western Ulleung Basin (Fig. 2b). After core splitting, macroscopic sedimentary structures and sediment color were described. X-radiographs in 1-cm thick slabs were taken to further describe sedimentary structures in detail. Three AMS $^{14}$C ages were determined on planktonic foraminifera collected in hemipelagic muds. These dating were performed at Beta Analytic Inc. (USA) and AMS Laboratory, University of Arizona (USA). Calendar ages were converted from radiocarbon ages using CALIB 7.1 (Stuiver et al., 2020). In order to compare lithologic characters and AMS $^{14}$C ages in the fan-shaped body to those in its outside area, core 07-1 (505 cm long) in Lee et al. (2013) was also used.

## 4. MORPHOLOGIC AND ACOUSTIC CHARACTERS

In the study area, a non-shelf indenting slope-failure system is present on the middle slope in water depths deeper than 600 m (Fig. 2a). The slope-failure system consists of several arcuate head (or main) scars with an area of ca. 117 km$^2$. The headwall scarps occur in water depths ranging between 600 and 850 m, and are up to about 60 m high. Several small-scale, elongated failure scars are present below the main scarps (Fig. 2a). These elongated scars are less than 5 km long and range from ca. 10 to 30 m in relief. The slope-failure system is connected downslope to a gully which reaches to the base-of-slope (Fig. 2a). The gully is about 2 km wide and 350 m deep in the proximal part, and its width gradually increases to the base-of-slope, with a concomitant decrease in its depth. Besides this gully, several small-scale gullies, not connected to the arcuate head scars on the middle slope, are present along the base-of-slope (Fig. 2a).

In MR-1 side-scan sonar images, a fan-shaped sedimentary body showing strong back-scatter intensity occurs at the base-of-slope, just downslope of the gully mouth (Fig. 2b). The fan-shaped body is less than about 10 km long in radius. The lateral boundary of the fan-shaped body is not clearly seen in the multi-beam bathymetry even though the water-depth contours on the fan-shaped body are slightly bulging outward (Fig. 2a). The fan-shaped body exhibits a convex-up, smooth surface morphology without distinct channel-levee systems (Figs. 2b, 3, and 4).

In Chirp (2–7 kHz) sub-bottom profiles crossing the fan-shaped body in MR-1 sonar images, two transparent masses are distinctly recognized at the base-of-slope (Figs. 3 and 4). The uppermost transparent mass is directly underlain by the interval


https://doi.org/10.1007/s12303-020-0008-9

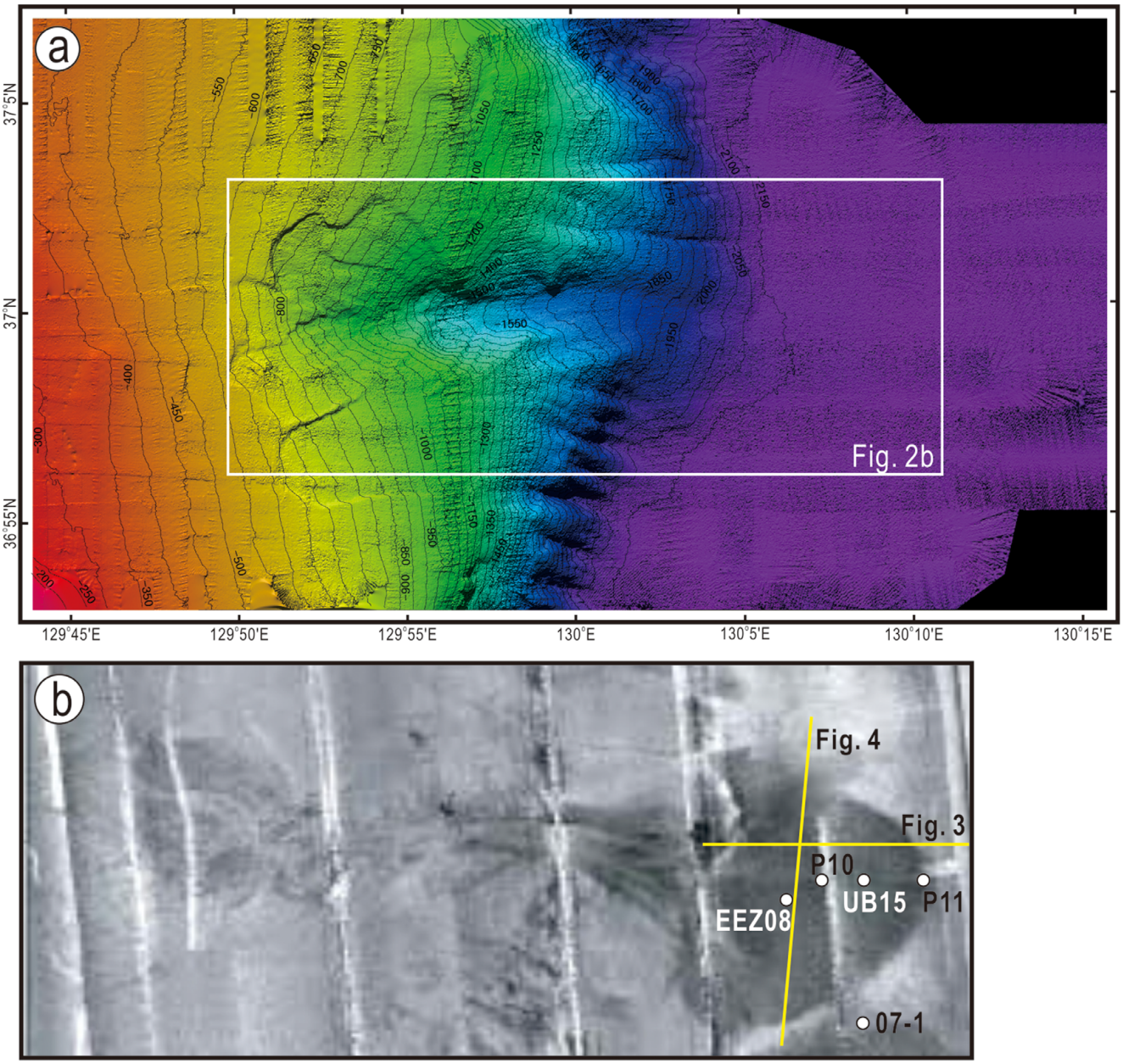


**Fig. 2.** (a) Bathymetric map showing morphologic features of a non-shelf indenting slope-failure system on the middle-to-lower slope from multi-beam echo sounding data. (b) MR-1 side-scan sonar images showing a strongly back-scattered, fan-shaped body at the base-of-slope. For location of Figures 2a and b, see Figures 1 and 2a, respectively.

of diffuse to distinct layers with a sharp or erosional contact (Figs. 3 and 4). Thickness of the uppermost transparent mass is ca. 20 m in the proximal part, and gradually decreases to the distal part in both longitudinal and transverse directions, forming a distinct lobe (Figs. 3 and 4). Below the interval of diffuse to distinct layers, the lower transparent mass is observed (Figs. 3 and 4).

## 5. SEDIMENTARY FACIES AND FACIES OCCURRENCES

On the basis of grain size and sedimentary structures, core sediments are classified into eleven sedimentary facies. Sedimentary features and interpretations of each facies are detailed in Table 1 and Figure 5. Sedimentary facies are grouped into 1) mass-transport deposits (MTDs), 2) turbidites, and 3) hemi-pelagic sediments. MTDs consist of five sedimentary facies; slightly distorted soft mud (facies SDM), moderately to highly distorted soft mud (facies MHDM), inhomogeneous, matrix-supported soft mud-clast gravel (facies IMG-a and IMG-b), and clast-supported, disorganized soft mud-clast gravel (facies CDG). These MTD facies are differentiated by the degree and type of soft-mud deformation (Table 1 and Figs. 5a–d). Turbidites comprise

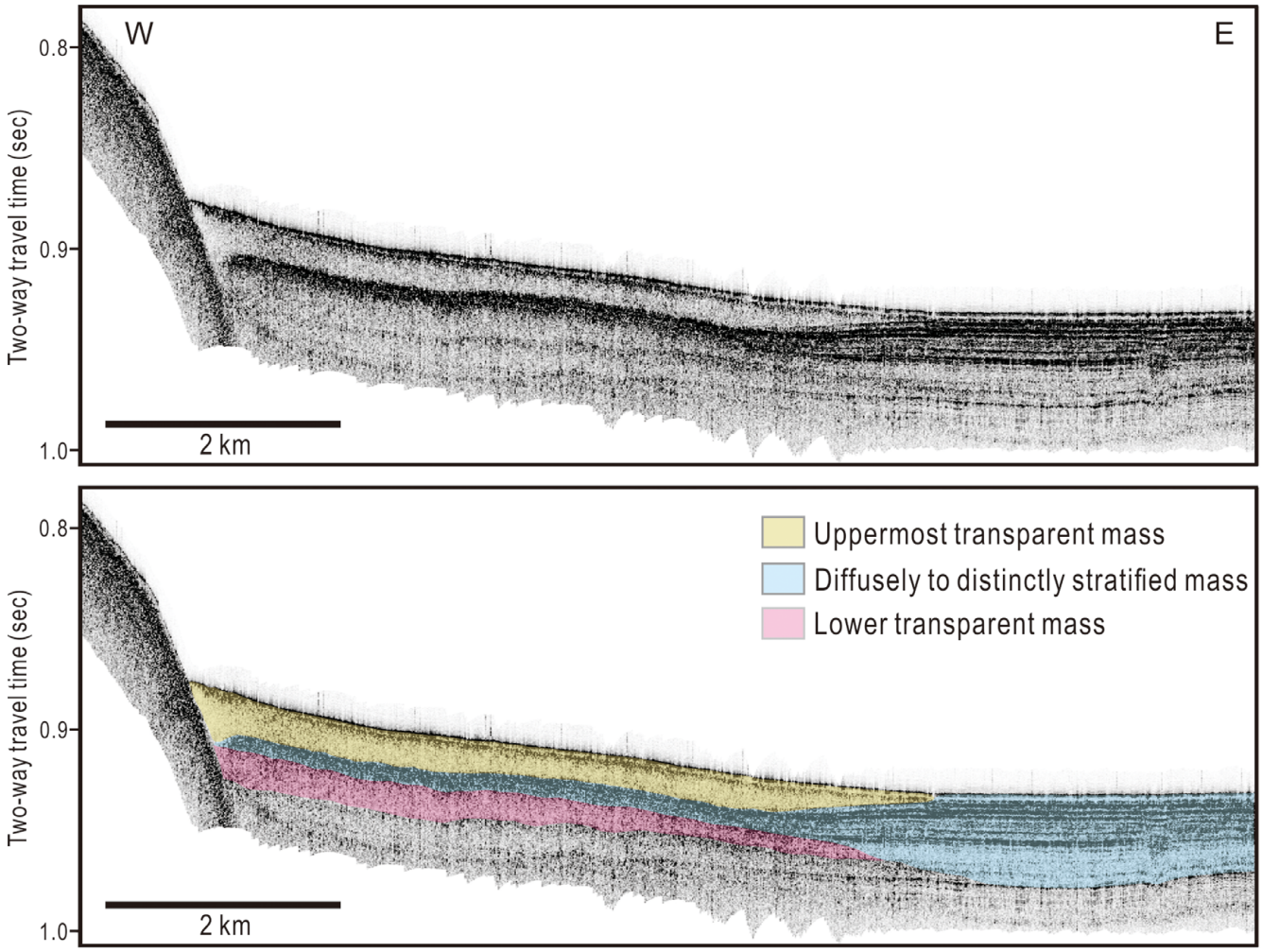


**Fig. 3.** High-resolution (Chirp, 2–7 kHz) sub-bottom profile (top) and interpreted section (bottom) longitudinally crossing the fan-shaped body in MR-1 sonar image. For location of Figure 3, see Figure 2b.

four sedimentary facies; massive sand (facies MS), laminated sand (facies LS), laminated mud (facies LM), and homogeneous mud (facies HM) (Table 1 and Figs. 5e and f). These sedimentary facies correspond to the classical turbidites of Bouma (1962), Piper (1978) and Lowe (1982). Hemi-pelagic sediments consist of crudely laminated mud (facies CLM) and bioturbated mud (facies BM) (Table 1 and Figs. 5f and g). Facies BM and CLM were deposited under oxygenated and poorly oxygenated bottom-water conditions in the East Sea, respectively (Bahk et al., 2000).

Four cores from the fan-shaped body in MR-1 sonar images (core EEZ08, P10, UB15, and P11 in Fig. 2b) exhibit MTD facies (facies SDM, MHDM, IMG-a, IMG-b, and CDG), just below ca. 1–2.2 m-thick, watery Holocene hemi-pelagic mud (facies BM) in the topmost part of each cores (Fig. 6). On the other hand, a core in the area outside the fan-shaped body (core 07-1 in Fig. 2b) does not include the MTD facies below the topmost, watery hemi-pelagic mud (facies BM) (core 07-1 in Fig. 6). The interval of the MTD facies in cores most likely corresponds to the uppermost transparent mass in Chirp sub-bottom profiles (Figs. 3 and 4). At the most distal area of the fan-shaped body (core P-11 in Fig. 2b), the interval of the MTD facies directly overlies the sequence of hemi-pelagic mud (facies CLM) and sandy/muddy turbidites (facies MS, LS, LM and HM) with a sharp contact (core P-11 in Fig. 6). The sequence of these turbidites and hemi-pelagic mud most likely corresponds to the diffusely to distinctly stratified mass below the uppermost transparent mass in Chirp sub-bottom profiles (Figs. 3 and 4).

The interval of the MTD facies below the surficial hemi-pelagic mud consists of two units without hemi-pelagic muds between them. The two units are interbedded only with a very thin (ca. 3-cm thick), fine-grained turbidite (facies LM and HM) at its most distal area of the fan-shaped body (core P-11 in Figs. 6 and 7). The upper unit is mostly occupied by facies CDG (clast-supported, disorganized soft-mud clast gravel) of which thickness is randomly variable from 25.3 to 127.3 cm in the longitudinal direction (Fig. 6). Mud clasts in facies CDG consist entirely of soft hemi-


https://doi.org/10.1007/s12303-020-0008-9

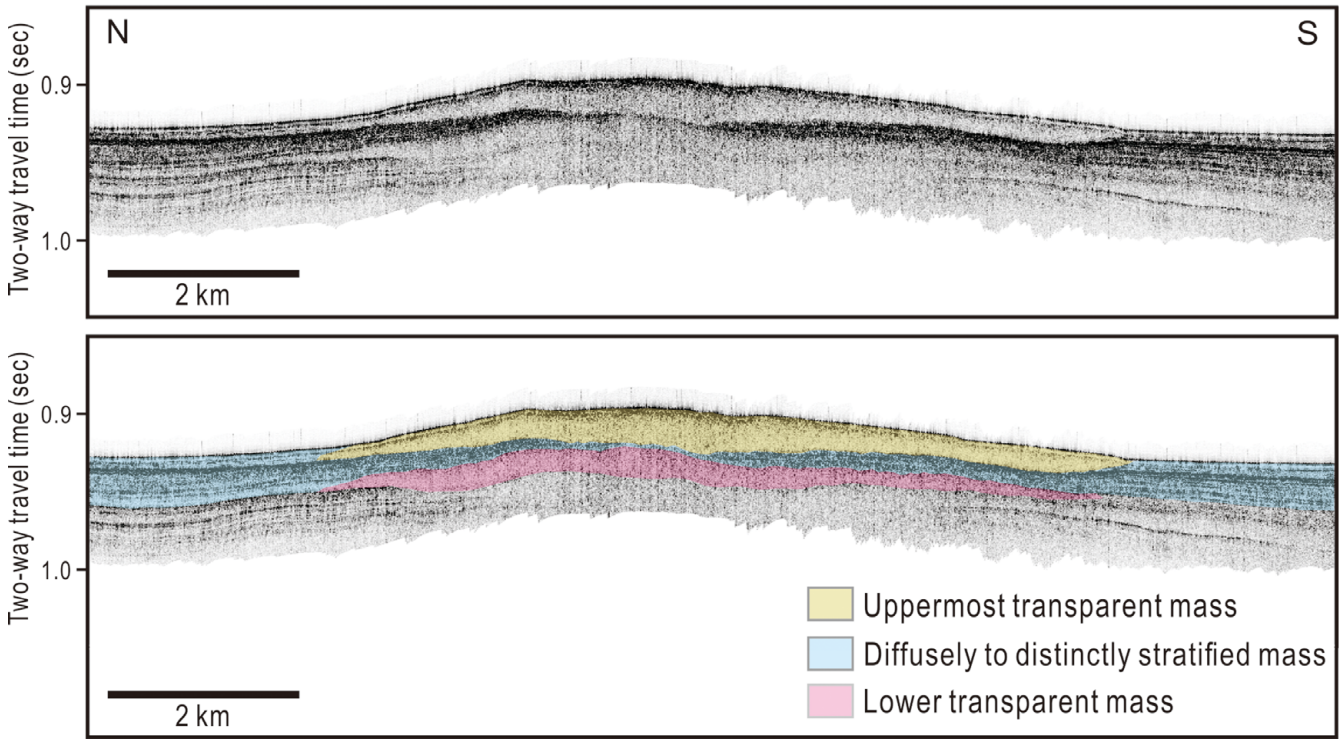


**Fig. 4.** Chirp (2–7 kHz) sub-bottom profile (top) and interpreted section (bottom) transversely crossing the fan-shaped body in MR-1 sonar images. For location of Figure 4, see Figure 2b.

pelagic muds (facies BM and CLM). In the proximal-to-middle area of the fan-shaped body, facies CDG is overlain by very thin (less than 1 cm thick), laminated sand (facies LS) which changes to medium-bedded (17.5 cm thick), laminated sand (facies LS) and homogeneous mud (facies HM) in its most distal area (Figs. 6 and 8).

The lower unit consists mostly of slightly to highly distorted soft mud (facies SDM and MHDM) associated with inhomogeneous, matrix-supported, soft mud-clast gravels (facies IMG-a and IMG-b) (Fig. 6). Facies SDM and MHDM range from about 10 to 110 cm in thickness, and the contact between these two facies is rather gradual. Muds in both facies SDM and MHDM consist of reworked soft hemi-pelagic muds (facies BM and CLM) subject to the deformation. AMS $^{14}$C ages of foraminifera in the slightly to highly distorted soft muds (facies SDM and MHDM) are older than 43,500 yrs B.P., that is beyond the limit of $^{14}$C dating (Table 2 and Fig. 6). Inhomogeneous, matrix-supported, soft mud-clast gravels (facies IMG-a and IMG-b) are generally bounded by slightly to highly distorted soft muds (facies SDM and MHDM) with gently to steeply inclined, distinct contact, and are 5.1–38.7 cm thick, relatively thinner than facies SDM and MHDM (Figs. 5b and c). Mud clasts in facies IMG-a and IMG-b also comprise soft hemi-pelagic muds (facies BM and CLM). In hemi-pelagic mud (facies CLM) just below the lower unit at the most distal area of the fan-shaped body, the calendar age of foraminifera converted from the AMS $^{14}$C age is about 17.0 cal. kyr B.P. (Table 2 and Fig. 6).

## 6. DISCUSSION

In the sonar images, acoustic back-scatter characteristics from deep-water terrigenous deposits have been widely used to recognize sediment type/distribution, seafloor morphology, or geometric features of sediment bodies (Masson et al., 1993; Migeon et al., 2010). The seafloor in the study area is mostly covered by ca. 1–2.5 m thick, watery Holocene hemi-pelagic mud (facies BM) in the topmost part of all cores (Fig. 6). The relatively thick (ca. 1–5 m) occurrences of the topmost, watery Holocene hemi-pelagic mud (facies BM) are unique in all areas of the slopes and basin plain of the Ulleung Basin (Bahk et al., 2000; Lee et al., 2004). Even though this Holocene hemi-pelagic mud drapes uniformly the seafloor, the strong back-scatter intensity of the fan-shaped body in the study area is clearly shown by the MR-1 sonar system (Fig. 2b). Back-scatter features are generally caused by the combination of the roughness and impedance contrast of the seafloor (i.e., surface scattering) and volume scattering from inhomogeneity in the shallow sub-bottom (Unterseh, 1999). Given that the signal frequency (11–12 kHz) and wavelength (12.5–13.6 cm) of the MR-1 system and the high water content of the topmost Holocene hemi-pelagic muds in the Ulleung

**Table 1.** Description and interpretation of sedimentary facies in core sediments

| Facies | Description | Interpretation |
|---|---|---|
| Slightly distorted soft mud (SDM) | Slightly distorted (or deformed) mud consisting of soft bioturbated (facies BM) or crudely laminated (facies CLM) muds; mostly, preservation of primary sedimentary structures (lamination and bioturbation); laminations or bedding layers: nearly horizontal to inclined up to 20°; vertical change in inclination of laminations or bedding layers; partly, very small-sized thin (less than 1 cm) lenticular or wavy bedding layers (or laminations); sometimes, very small-scale (1–3 cm thick) internal faults (displacement: less than 0.5 cm) and folds (s- or v-shaped) with some micro-flame structures; commonly associated with facies MHDM, IMG-a and IMG-b; 13.5–110.5 cm thick | Brittle or low-degree plastic deformation of soft hemi-pelagic muds (facies BM and CLM) |
| Moderately to highly distorted soft mud (MHDM) | Moderately to severely folded or convoluted mud consisting of soft bioturbated (facies BM) and crudely laminated (facies CLM) muds; either destruction or partial preservation of primary sedimentary structures (lamination and bioturbation); some inclined, lens-shaped (lenticular) layers; commonly associated with facies SDM, IMG-a and IMG-b; 10.0–39.2 cm thick | High-degree plastic deformation of soft hemi-pelagic muds (facies BM and CLM) with partial liquefaction |
| Inhomogeneous, matrix-supported soft mud-clast gravel (IMG-a and IMG-b) | Inhomogeneous, mud-matrix-supported soft mud clasts consisting of bioturbated (facies BM) and crudely laminated (facies CLM) muds; according to the orientation pattern of matrix zone, subdivided into IMG-a and IMG-b; some intervals exhibiting transitional sedimentary features between IMG-a and IMG-b | Strong shearing and plastic mixing of soft hemi-pelagic muds (facies BM and CLM) |
| | IMG-a<br>Orientation of matrix zone: nearly parallel to each other within the unit, forming one dominant orientation pattern; nearly horizontal to inclined matrix zone; in the matrix zone, common occurrence of strongly sheared fabric or lineation; mud clast: very elongated shape, (nearly) parallel to sheared fabric/lineation in the matrix zone; smooth to irregular surface; less than 4-5 cm long, common deformation of primary structures in the clasts; common alternation with facies IMG-b; mostly associated with facies IMG-b, SDM and MHDM; generally, 5.112.0 cm thick, but when the transitional sedimentary features between facies IMG-a and IMG-b are present, thickness ranges from 23.3 to 27.1 cm | |
| | IMG-b<br>Random orientation of matrix zone; less sheared fabric and lineation in the matrix zone compared to facies IMG-a; various shapes of mud clasts with smooth to irregular surface; various orientation of mud clasts; common deformation of primary sedimentary structures in the mud clasts; clast size: 3-16 cm long, larger than those in facies IMG-a; some mud clasts showing zig-saw shape pattern to the adjacent ones with common filling of mud matrix between the clasts; mostly associated with facies IMG-a and SDM; 17.9-38.7 cm thick | |
| Clast-supported, disorganized soft mud-clast gravel (CDG) | Clast-supported, randomly oriented, soft mud clasts consisting of bioturbated (facies BM) and crudely laminated (facies CLM) muds; overall, ungraded mud clasts with partly inverse grading in the basal part; pebble- to cobble-sized (0.7–9 cm long) mud clasts; various shape of mud clasts from sub-angular to well rounded; irregular surface of mud clasts; slight to severely deformation of primary sedimentary structures in the clasts; commonly associated with facies IMG-a, SDM, LS, HM and BM; 25.3–127.3 cm thick | En-mass freezing (low-viscous debris flow) from extensive breaking up of soft hemi-pelagic muds (facies BM and CLM) |
| Massive sand (MS) | Moderately sorted, massive sand (sand contents 80–90%); sand fraction: mostly, fine-sand graded, terrigenous materials and foraminifera; mostly associated with facies LS and HM; 23.2 cm thick | Rapid suspension or continuous aggradation from high-/low-density turbidity currents (Lowe, 1982) |
| Laminated sand (LS) | Faintly to well laminated sand and silty sand; horizontal to slightly inclined laminations; an upward decrease in frequency and thickness of sand laminae; sand fractions: mostly fine-sand graded, foraminifera with some terrigenous materials; underlain by facies CDG, CLM and MS with either distinct or gradational contacts; overlain by facies LM and HM with distinct to indistinct contacts; less than 10 cm thick | $T_c$ or $T_d$ division of Bouma (1962) |
| Laminated mud (LM) | Faintly to well laminated mud; horizontal or slightly inclined laminations; alternation of silt and clay laminations less than a few millimeters thick; generally, an upward decrease in frequency and thickness of silt laminae; mostly underlain by facies LS and HM with gradual contact; commonly overlain by facies HM with gradual contact; sometimes, alternation of facies LM and HM; 3.1 to 21.4 cm in thickness | $E_1$ (laminated mud) division of fine-grained turbidites of Piper (1978) |
| Crudely laminated mud (CLM) | Generally, dark olive mud; horizontally crude laminations on X-radiographs; no systematically vertical variation in clarity and thickness of laminations; sand fractions: well preserved planktonic foraminifera used for AMS $^{14}C$ dating; generally associated with facies HM and BM; sometimes, overlain by facies MHDM and LS with sharp (erosive), irregular-relief contacts; variable in thickness from 1.3 to 10.2 cm | Hemi-pelagic sedimentation under poorly oxygenated bottom-water conditions (Bahk et al., 2000) |
| Homogeneous mud (HM) | Usually, light olive gray mud; on X-radiographs, lacks visible primary sedimentary structures, but often shows very faint or diffuse, horizontal to slightly inclined laminations; underlain by LM and LS with gradual contact and facies CLM with distinct boundary; overlain by BM, CLM, MS and CDG with either distinct or indistinct boundaries; variable in thickness from 2.3 to 63 cm | Graded ($E_2$)/ungraded ($E_3$) mud of fine-grained turbidites of Piper (1978) |
| Bioturbated mud (BM) | Indistinctly to distinctly burrowed or bioturbated mud; partly, diffuse (or crudely) laminations disturbed by bioturbation; generally light gray in color; over 70% of clay; variable in thickness from 4.5 to 219 cm | Hemi-pelagic settling under oxygenated bottom-water conditions (Bahk et al., 2000) |


https://doi.org/10.1007/s12303-020-0008-9

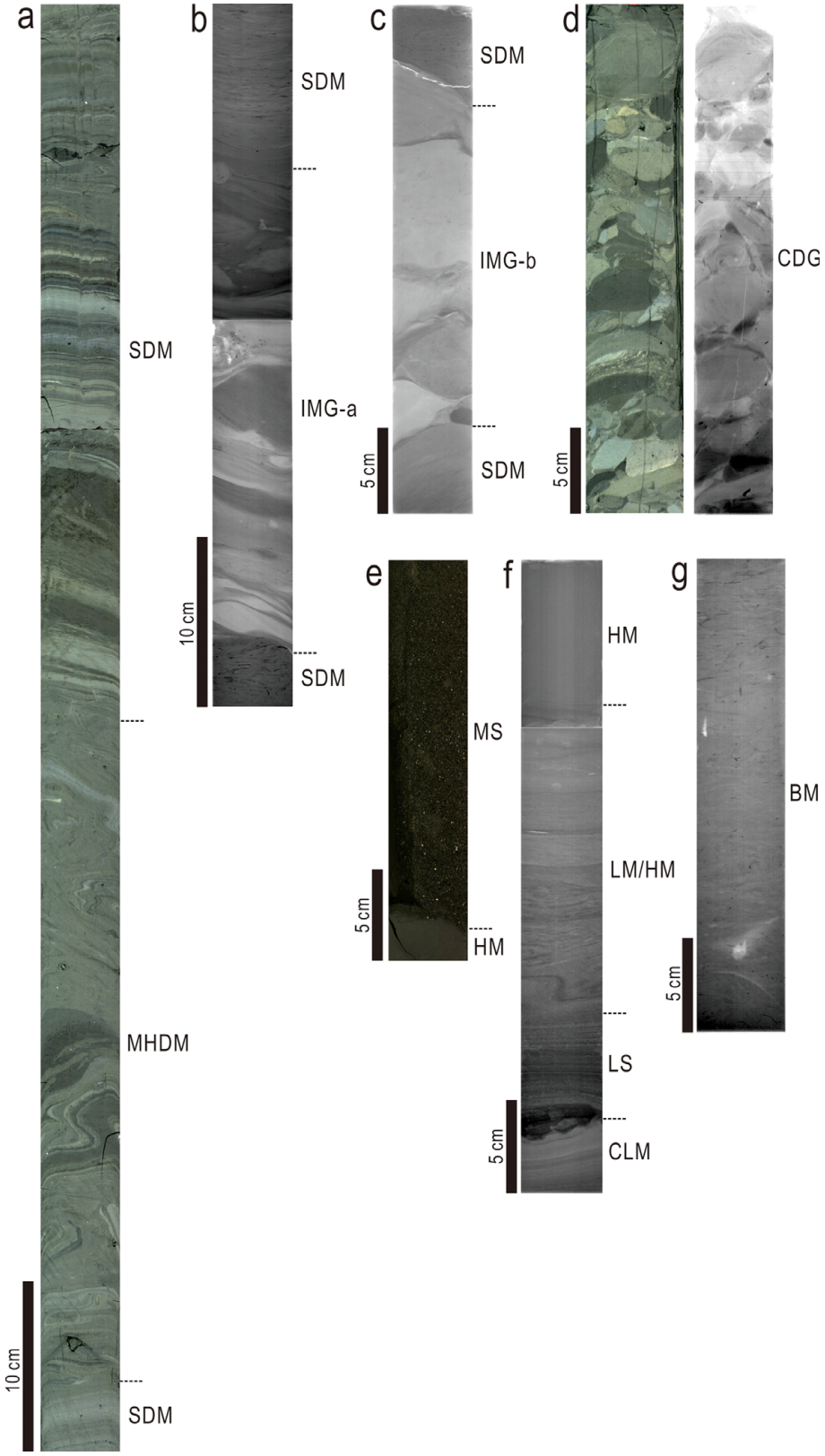


**Fig. 5.** Core photographs (a, d-left and e) and x-radiographs (b, c, d-right, f and g) of sedimentary facies. BM = bioturbated mud; CDG = clast-supported, disorganized soft mud-clast gravel; CLM = crudely laminated mud; HM = homogeneous mud; IMG-a/-b = inhomogeneous, matrix-supported soft mud-clast gravel-a/-b; LM = laminated mud; LS = laminated sand; MHDM = moderately to highly distorted soft mud; MS = massive sand; SDM = slightly distorted soft mud. For location of photographs and x-radiographs, see Figure 6.

Basin, acoustic signals of the MR-1 system can usually penetrate sediments up to several meters below the seafloor (Lee et al., 2013). Considering the thickness of the uppermost transparent mass and the underlying stratified sediments in Chirp sub-bottom profiles (Figs. 3 and 4), the lower transparent mass in Chirp sub-bottom profiles most likely does not contribute to the strong

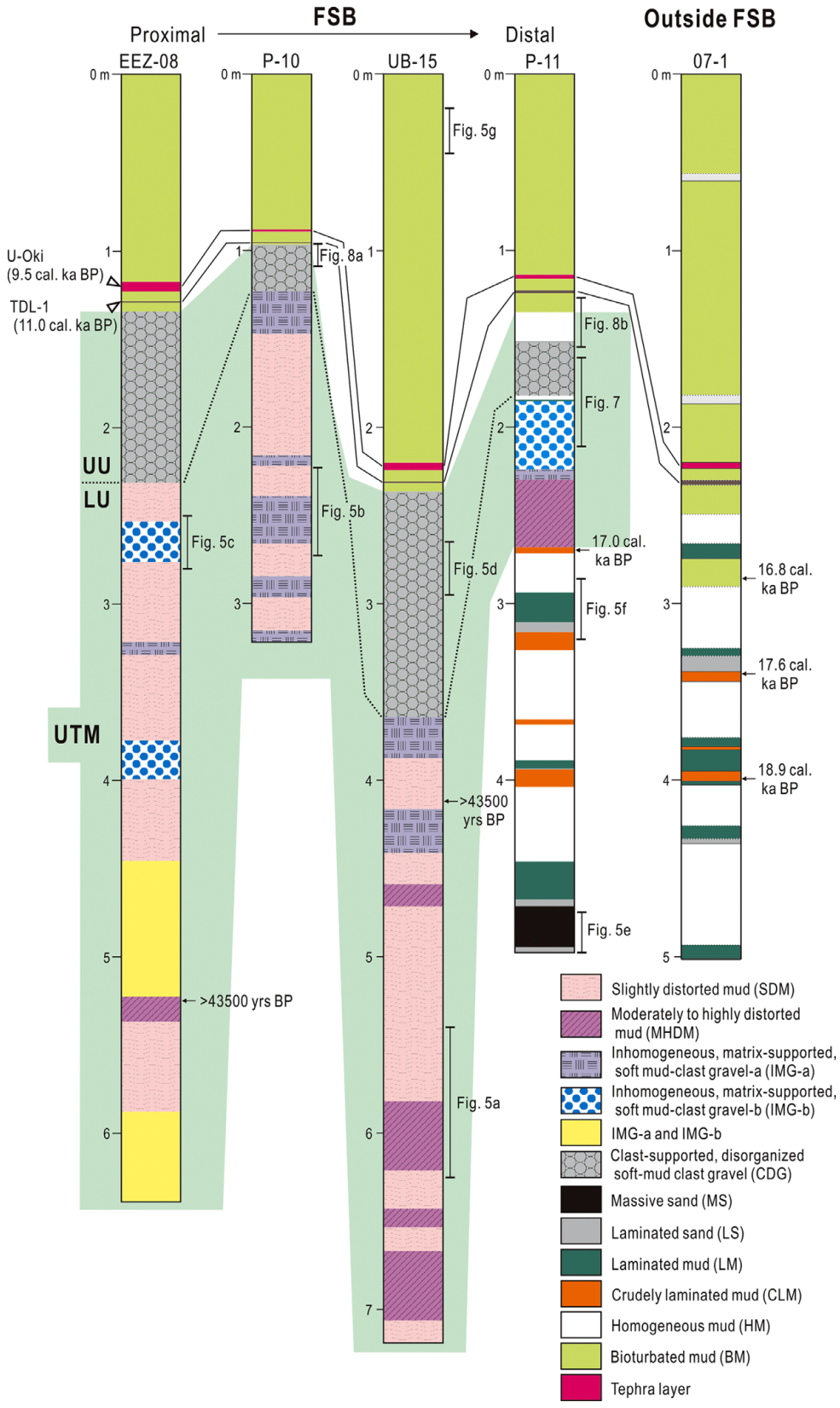


**Fig. 6.** Sedimentary logs and correlation of sediment cores. Open triangles on the left side indicate the ages of the U-Oki (Ulleung-Oki) tephra layer and TDL (thin, dark layer)-1 from Machida (1999), Miyairi et al. (2004) and Lee (2007). Arrows with number on the right side represent the ages from foraminifera. FSB = fan-shaped body in MR-1 sonar images; LU = lower unit of the MTD facies interval; UTM (area of mint green) = uppermost transparent mass in Chirp sub-bottom profiles; UU = upper unit of the MTD facies interval. Bars on the right side indicate the location of Figures 5, 7, and 8. For location of cores, see Figure 2b.


https://doi.org/10.1007/s12303-020-0008-9

**Table 2.** AMS $^{14}$C ages of planktonic foraminifera

| Core No. | Depth (cm) | Lab No. | AMS $^{14}$C ages (yr BP) | Calendar ages[(a)] (cal yr BP) |
|---|---|---|---|---|
| EEZ-08 | 523 | Beta-463533 | > 43500 | |
| UB-15 | 412–414 | Beta-462719 | > 43500 | |
| P-11 | 270–272 | B10881 | 14436 ± 48 | 17054 ± 204 |

[(a)]Calendar ages converted from radiocarbon ages using CALIB 7.0.4 (Stuiver et al., 2018).

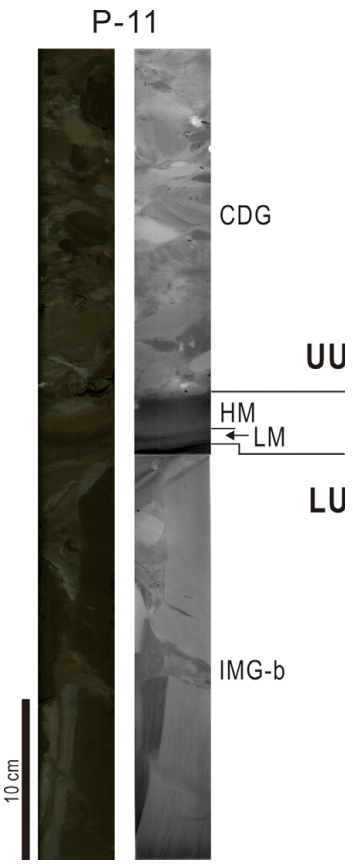


**Fig. 7.** Photograph (left) and x-radiograph (right) of very thin fine-grained turbidites (facies LM and HM) intervened between the lower and upper units of the upper transparent mass (UTM) at the most distal area of the fan-shaped body in MR-1 sonar images. CDG = clast-supported, disorganized soft mud-clast gravel; HM = homogeneous mud; IMG-b = inhomogeneous, matrix-supported soft mud-clast gravel; LM = laminated mud; LU = lower unit of the UTM; UU = upper unit of the UTM. For location of photograph and x-radiograph, see Figure 6.

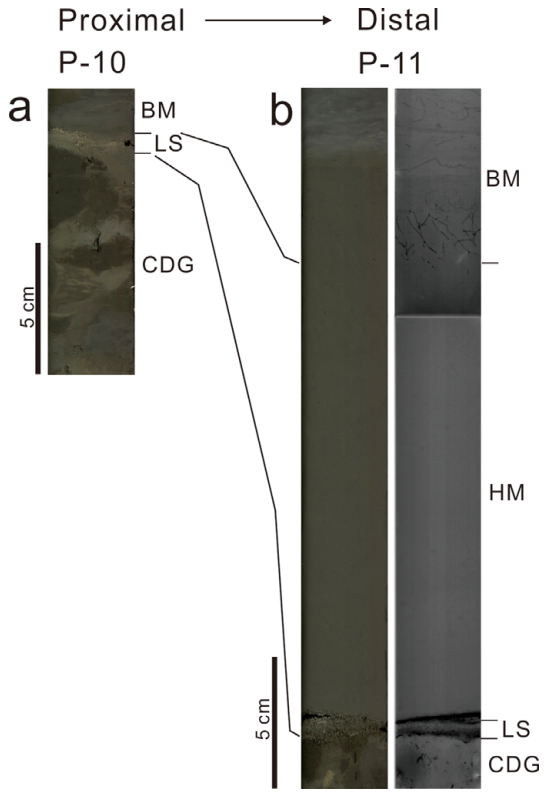


**Fig. 8.** Photographs (a and b-left) and x-radiograph (b-right) of facies LS and HM overlying facies CDG in the upper unit of the upper transparent mass. CDG = clast-supported, disorganized soft mud-clast gravel; HM = homogeneous mud; LS = laminated sand. For location of photographs and x-radiograph, see Figure 6.

back-scatter intensity of the fan-shaped body in the sonar images. The strong back-scatter intensity of the fan-shaped body in MR-1 sonar images could be ascribed to the interval of MTD facies (facies CDG, SDM, MHDM, IMG-a, and IMG-b) in core sediments. The fan-shaped body in the sonar images can therefore be considered to exactly reflect the uppermost transparent mass in Chirp sub-bottom profiles.

Between the lower and upper units of the MTD facies interval, the absence of hemi-pelagic muds only with an interlayer of very thin (ca. 3 cm thick) fine-grained turbidite (facies LM and HM) at the most distal area implies that the upper unit was subsequently deposited after formation of the lower unit without a significant time break. The interval of MTD facies could be, therefore, considered to be deposited during a single event (e.g., Hunt et al., 2011; Gladstone et al., 2018). The laterally wedged, acoustically transparent characters without the stratified intervals in high-resolution sub-bottom profiles further indicate that the fan-shaped body was most likely deposited during the same event, although such event could have been separated in at least two stages (Fig. 9).

In the lower unit, the strongly sheared and relatively thin (mostly less than ca. 20–30 cm thick) IMG-a and IMG-b facies (inhomogeneous, matrix-supported, soft-mud clast gravels) most likely represent very strong deformation zones (Tripsanas et al., 2008; Bahk et al., 2017). Slightly to highly distorted soft muds (facies SDM and MHDM) associated with facies IMG-a

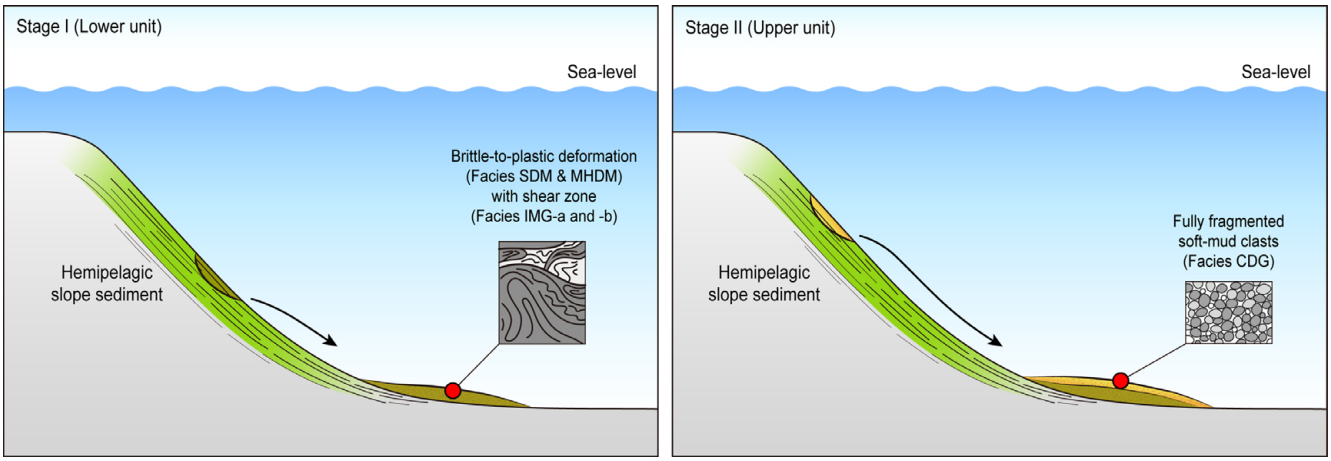


**Fig. 9.** A schematic diagram (not to scale) illustrating the mass-transport processes and possible failing areas of the lower and upper unit in the fan-shaped body which formed during a single event separated in two stages without a significant time break. CDG = clast-supported, disorganized soft mud-clast gravel; IMG-a/-b = inhomogeneous, matrix-supported soft mud-clast gravel-a/-b; MHDM = moderately to highly distorted soft mud; SDM = slightly distorted soft mud.

and IMG-b are mostly indicative of less deformed intervals, such as small-scale mud blocks or mud clasts, between the strongly shearing zones (facies IMG-a and IMG-b) in the MTDs (Martinsen, 1994; Lee and Stow, 2007; Tripsanas et al., 2008; Bahk et al., 2017). These features suggest that the lower unit could be deposited by either slides/slumps or high-viscous debris flows (Hampton et al., 1996; Mulder and Cochonat, 1996; Tripsanas et al., 2008). $^{14}$C ages of foraminifera in the lower unit suggest that the sediments reworked by the slope failure are older than at least 43,500 yrs B.P. Very small-scale, residual turbidity currents, immediately following the deposition of the lower unit, most likely formed the very thin (ca. 3 cm thick), fine-grained turbidites (facies LM and HM) on the most distal area of the MTD fan.

In the upper unit, the clast-supported, randomly-oriented, pebble-to-cobble sized (0.7–9 cm long) soft hemi-pelagic mud clasts of facies CDG indicate that the soft hemi-pelagic mud was extensively broken up during the transport (Tripsanas et al., 2008; Bahk et al., 2017). The ungraded and clast-supported structures of facies CDG suggest that the upper unit was most likely deposited by low-viscous debris flows (Mulder and Cochonat, 1996; Lee et al., 2013). The random variation in thickness of facies CDG in the longitudinal direction implies that the debris flows were most likely deposited upon the inherently irregular-undulated upper surface of the lower unit formed by slides/slumps or high-viscous debris flows (e.g., Masson et al., 1993, 1997; Lee et al., 1999). The residual turbidity currents associated with the debris flows probably deposited the thin fine-grained turbidite (facies LS and HM) overlying facies CDG.

The original lithology of the upper and lower units before the resedimentation (i.e., slope failure) is the same (i.e., soft hemi-pelagic mud). This original lithology is well matched with soft hemi-pelagic muds from sediment cores (ca. 3–11 m long) in the undisturbed areas around the isolated slope-failure system (Lee et al., 2014; Cukur et al., 2016), suggesting that the original lithology had a minor role in the different depositional regimes (or processes) between the upper and lower units. The contrast in depositional processes between two units could therefore be ascribed to different downslope transportation styles during the same landslide event. Compared to brittle to plastic deformation (internal folds and faults) of soft hemi-pelagic mud in the lower unit, the full fragmentation of soft hemi-pelagic mud clasts in the upper unit implies that the upper unit underwent more shearing during the downslope movement than the lower units. Considering the small dimension of the fan-shaped body and slope-failing system and the same original lithology between two units, the more shearing in the upper unit is most likely suggestive of longer transport distance of the upper unit that that of the lower unit (Fig. 9). Alternatively, the brittle to plastic deformation (internal folds and faults) of soft hemi-pelagic mud in the lower unit (or a fraction of it) could be probably caused by shearing and loading of the overlying debris flows (i.e., the upper unit) onto the fine-grained (muddy) basin plain sediments. In the Ulleung Basin, sediment cores (less than 10 m long) from the basin plain mostly include a certain interval (at least ca. 20–30% in core length) of fine-grained turbidites (thinly laminated sand, laminated mud, and homogeneous mud) (core 07-1 in Fig. 6; Bahk et al., 2000; Lee et al., 2004). However, the lower unit does not exhibit the deformed fine-grained turbidites. This alternative interpretation can be rule out.

Submarine gully and canyon have known to be generally formed by either slope failures or erosion associated with turbidity currents (Pratson and Coakley, 1996; Saller et al., 2012). The fan-shaped body in the study area is mostly occupied by slides/slumps and debris-flow deposits (MTDs) with rare turbidites. It has a convex-


https://doi.org/10.1007/s12303-020-0008-9

up, smooth surface morphology without distinct channel-levee systems. The fan-shaped body connects to the small-scale gully bounded upslope by failure scars confined in the upper to middle slopes. These morphologic and sedimentary features imply that the submarine gully in the study area could mostly formed by slope failures, not by erosion of turbidity currents.

## 7. CONCLUSIONS

A slope-failure system (ca. 117 $km^2$ in area) not directly connected to the shelf break is present in water depths exceeding 600 m in the western margin of the Ulleung Basin. It consists of several arcuate head scars with the main scarp being up to ca. 60 m high. The slope-failure system is connected downslope to a gully and fan-shaped body at the base-of-slope. The fan-shaped body, less than ca. 10 km long in radius, is characterized by strong back-scatter intensity in MR-1 sonar images. Considering the acoustic penetration depth (up to several meters) of the MR-1 sonar system, it exactly corresponds to the uppermost transparent mass in Chirp sub-bottom profiles. Sediment cores penetrating to the uppermost transparent mass consist mostly of MTD facies (facies CDG, SDM, MHDM, IMG-a, and IMG-b), most likely causing the strong back-scatter intensity of the fan-shaped body. The interval of the MTD facies comprises two units (upper and lower) without hemi-pelagic muds between them. The two units are intervened only with a very thin (ca. 3 cm thick) fine-grained turbidite at the most distal area of the fan-shaped body, suggesting that the fan-shaped body formed during a single event separated in at least two stages without a significant time break. The upper unit is characterized by fully fragmented soft hemi-pelagic mud clasts (facies CDG) formed by low-viscous debris flows. On the other hand, the lower unit shows brittle to plastic deformation (internal folds and faults) of soft hemi-pelagic mud (facies SDM and MHDM) associated with thin shear zone (facies IMG-a and IMG-b), most likely formed by slides/slumps or high-viscous debris flows. Both the upper and lower units display the same original lithology (soft hemi-pelagic mud) prior to the failure, indicating that the lithology could not significantly affect different depositional regimes between two units. Compared to the brittle to plastic deformation of soft mud in the lower unit, the full fragmentation of soft mud clasts in the upper unit implies that the upper unit underwent more shearing during the downslope transport than the lower unit. Under the small dimension of the fan-shaped body and the slope-failing system, the more shearing in the upper unit could be ascribed to longer transport distance than that of the lower unit. The rare turbidites with absence of channel-levee systems in the fan-shaped body and the failure scars confined in the upper to middle slopes suggest that the submarine gully probably formed by slope failures, not by erosion of turbidity currents.

## ACKNOWLEDGMENTS

This study is supported by Project of the KIOST (PE99741) and KIGAM (GP2017-21). JJ Bahk is supported by research fund of Chungnam National University. We greatly thank SH Lee, CK Jeon, CH Kim, HJ Moon, and SH Ahn for making figures and maps.

## REFERENCES

Bahk, J.J., Chough, S.K., and Han, S.J., 2000, Origins and paleoceanographic significance of laminated muds from the Ulleung Basin, East Sea (Sea of Japan). Marine Geology, 162, 459–477.

Bahk, J.J., Kang, N.K., Yi, B.Y., Lee, S.H., Jeong S.W., Urgeles, R., and Yoo, D.G., 2017, Sedimentary characteristics and processes of submarine mass-transport deposits in the Ulleung Basin and their relations to seismic and sediment physical properties. Marine Geology, 393, 124–140.

Bouma, A.H., 1962, Sedimentology of Some Flysch Deposits. Elsevier, Amsterdam, 168 p.

Chough, S.K., Lee, S.H., Kim, J.W., Park, S.C., Yoo, D.G., Han, H.S., Yoon, H.S., Oh, S.B., Kim, Y.B., and Back, G.G., 1997, Chirp (2–7 kHz) echo characters in the Ulleung Basin. Geosciences Journal, 1, 143–153.

Cukur, D., Kim, S.P., Kong, G.S., Bahk, J.J., Horozal, S., Um, I.K., Lee, G.S., Chang, T.S., Ha, H.J., Völker, D., and Kim, J.K., 2016, Geophysical evidence and inferred triggering factors of submarine landslides on the western continental margin of the Ulleung Basin, East Sea. Geo-Marine Letters, 36, 425–444.

Elverhoi, A., Breien, H., de Blasio, F.V., Harbitz, C.B., and Pagliardi, M., 2010, Submarine landslides and the importance of the initial sediment composition for run-out length and final deposit. Ocean Dynamics, 60, 1027–1046.

Hampton, M.A., Lee, H.J., and Locat, J., 1996, Submarine landslides. Reviews of Geophysics, 34, 33–59.

Hunt, J.E., Wynn, R.B., Masson, D.G., Talling, P.J., and Teagle, D.A.H., 2011, Sedimentological and geochemical evidence for multistage failure of volcanic island landslides: a case study from Icod landslide on north Tenerife, Canary Islands. Geochemistry, Geophysics, Geosystems, 12, Q12007. https://doi.org/10.1029/2011GC003740

Gardner, J.M, Shor, A.N., and Jung, W.Y., 1998, Acoustic imagery evidence for methane hydrates in the Ulleung Basin. Marine Geophysical Researches, 20, 495–503.

Gladstone, C., McClelland, H.L.O., Woodcock, N.H., Pritchard, D., and Hunt, J.E., 2018, The formation of convolute lamination in mud-rich turbidites. Sedimentology, 65, 1800–1825.

Lee, K.E., 2007, Surface water changes recorded in Late Quaternary marine sediments of the Ulleung Basin, East Sea (Japan Sea). Palaeogeography, Palaeoclimatology, Palaeoecology, 247, 18–31.

Lee, S.H. and Stow, D.A.W., 2007, Laterally continuous, concave-up basal shear surfaces of submarine landslide deposits (Miocene), southern Cyprus: differential movement of sub-blocks within a single submarine landslide lobe. Geosciences Journal, 11, 315–321.

Lee, S.H., Chough, S.K., Back, G.G., Kim, Y.B., and Sung, B.S., 1999, Gradual downslope change in high-resolution acoustic characters and geometry of large-scale submarine debris lobes in Ulleung Basin, East Sea (Sea of Japan), Korea. Geo-Marine Letters, 19, 254–161.

Lee, S.H., Bahk, J.J., and Chough, S.K., 2004, Late Quaternary sedimentation in the eastern continental margin of the Korean Peninsula. In: Clift, P., Kuhnt, W., Wang, P., and Hayes, D. (eds.), Continent-Ocean Interactions within East Asian Marginal Seas. American Geophysical Union, Geophysical Monograph, 149, p. 205–233.

Lee, S.H., Jung, W.Y., Bahk, J.J., Gardner, J.M., Kim, J.K., and Lee, S.H., 2013, Depositional features of co-genetic turbidite-debrite beds and possible mechanisms for their formation in distal lobated bodies beyond the base-of-slope, Ulleung Basin, East Sea (Japan Sea). Marine Geology, 346, 124–140.

Lee, S.H., Bahk, J.J., Kim, H.J., Kim, G.Y., Kim, S.P., Jeong, S.W., and Park, S.H., 2014, Contrasting development of the Latest Quaternary slope failures and mass-transport deposits in the Ulleung Basin, East Sea (Japan Sea). In: Kraste, S., Behrmann, J.H., Völker, D., Stipp, M., Berndt, C., Urgeles, R., Chaytor, J., Huhn, K., Strasser, M., and Harbitz, C.B. (eds.), Submarine Mass Movements and Their Consequences. Advances in Natural and Technological Hazards Research, 37, p. 403–412.

Locat, J. and Lee, H.J., 2002, Submarine landslides: advances and challenges. Canadian Geotechnical Journal, 39, 193–212.

Lowe, D.R., 1982, Sediment gravity flows; II, depositional models with special reference to the deposits of high-density turbidity currents. Journal of Sedimentary Research, 52, 279–297.

Machida, H., 1999, The stratigraphy, chronology and distribution of distal marker-tephras in and around Japan. Global Planetary Change, 21, 71–94.

Martinsen, O., 1994, Mass movements. In: Maltman, A. (ed.), The Geological Deformation of Sediments. Chapman & Hall, London, p. 127–165. https://doi.org/10.1007/978-94-011-0731-0_5

Masson, D.G., Huggett, Q.J., and Brunsden, D., 1993, The surface texture of the Saharan Debris Flow deposit and some speculations on submarine debris flow processes. Sedimentology, 40, 583–598.

Masson, D.G., van Niel, B., and Weaver, P.P.E., 1997, Flow processes and sediment deformation in the Canary Debris Flow on the NW African continental rise. Sedimentary Geology, 110, 163–179.

Masson, D.G., Watts, A.B., Gee, M.J.R., Urgeles, R., Mitchell, N.C., Le Bas, T.P., and Canals, M., 2002, Slope failures on the flanks of the western Canary Islands. Earth-Science Reviews, 57, 1–35.

Masson, D.G., Harbitz, C., B., Wynn, R.B., Pedersen, G., and Lovholt, F., 2006, Submarine landslides: processes, triggers and hazard prediction. Philosophical Transactions of the Royal Society A, 364, 2009–2039.

McAdoo, B.G., Pratson, L.F., and Orange, D.L., 2000, Submarine landslide geomorphology, US continental slope. Marine Geology, 169, 103–136.

Migeon, S., Ducassou, E., Le Gonidec, Y., Rouillard, P., Mascle, J., and Revel-Rolland, M., 2010, Lobe construction and sand/mud segregation by turbidity currents and debris flows on the western Nile deep-sea fan (Eastern Mediterranean). Sedimentary Geology, 229, 124–143.

Miyairi, Y., Yoshida, K., Miyazaki, Y., Matsuzaki, H., and Kaneoka, I., 2004, Improved $^{14}C$ dating of a tephra layer (AT tephra, Japan) using AMS on selected organic fractions. Nuclear Instruments and Methods in Physics Research Section B, 223, 555–559.

Mulder, T. and Cochonat, P., 1996, Classification of offshore mass movements. Journal of Sedimentary Research, 66, 43–57. https://doi.org/10.1306/D42682AC-2B26-11D7-8648000102C1865D

Piper, D.J.W., 1978, Turbidite muds and silts in deep-sea fans and abyssal plains. In: Stanley, D.J. and Kelling, G. (eds.), Sedimentation in Submarine Fans, Canyons, and Trenches. Dowden, Hutchison and Ross, Stroudsburg, p. 163–176.

Piper, D.J.W., Farre, J.A., and Shor, A., 1985, Late Quaternary slumps and debris flows on the Scotian slope. Geological Society of America of Bulletin, 96, 1508–1517.

Piper, D.J.W., Cochonat, P., and Morrison, M.L., 1999, The sequence of events around the epicentre of the 1929 Grand Banks earthquake: initiation of debris flows and turbidity current inferred from sidescan sonar. Sedimentology, 46, 79–97.

Pratson, L.F. and Coakley, B.J., 1996, A model for the headward erosion of submarine canyons induced by downslope-eroding sediment flow. Geological Society of America Bulletin, 108, 225–234.

Saller, A. and Dharmasamadhi, I., 2012, Controls on the development of valleys, canyons, and unconfined channel-levee complexes on the Pleistocene Slope of East Kalimantan, Indonesia. Marine and Petroleum Geology, 29, 15–34.

Stuiver, M., Reimer, P.J., and Reimer, R.W., 2020, CALIB 7.1 WWW program at http://calib.org [Accessed on 19 April 2020].

Tripsanas, E., Piper, D.J.W., Jenner, K.A., and Bryant, W.R., 2008, Submarine mass-transport facies: new perspectives on flow processes from cores on the eastern North American margin. Sedimentology, 55, 97–136. https://doi.org/10.1111/j.1365-3091.2007.00894.x

Unterseh, S., 1999, Cartographie et caractérisation du fond marin par sondeur multifaisceaux. Institut Nationale Polytechnique de Lorraine, Nancy, 234 p.

Walker, R.G., 1992, Turbidites and submarine fans. In: Walker, R.G. and James, N.P. (eds.), Facies Models: Response to Sea Level Change. Geological Association of Canada, p. 239–263.





https://doi.org/10.1007/s12303-020-0008-9